


Simulation of virus-laden droplets transmitted from lung to lung

Shohei Kishi¹, Yuta Ida¹, Masashi Yamakawa¹^[0000-0001-5960-2602] and Momoha Nishimura¹^[0000-0002-7727-4566]

¹ Kyoto Institute of Technology, Matsugasaki, Sakyo-ku, Kyoto 606-8585, Japan
sk2.090412066@gmail.com

Abstract. In this study, we conducted a computational fluid dynamics analysis to estimate the trajectory of the virus-laden droplets. As numerical models, two human body models with airways were prepared. These models are represented by unstructured grids. Having calculated the unsteady airflow in the room, we simulated the trajectory of droplets emitted by the human speaking. In addition, inhaling the droplets into the lung of the conversation partner was simulated. The number of the droplets adhered to the respiratory lining of the partner was counted separately on the nasal cavity, oral cavity, trachea, bronchi, and bronchial inlet surface. The diameters of the droplets were also investigated in the same manner. It was noticeable that more than 80% of the droplets inhaled by the conversation partner adhered to the bronchial inlet surface. Also, the conversation partner did not inhale droplets larger than $35\mu\text{m}$ in diameter. It was found that when the distance between two people was 0.75m, more droplets adhered to the partner's torso.

Keywords: COVID-19, Respiratory organ, Computational fluid dynamics

1 Introduction

The global spread of COVID-19 revealed a lack of conventional knowledge about airborne infections. In fact, it is only in recent years that research about the mechanisms of airborne infection has been a focus of attention. Therefore, the airborne transmission route of COVID-19 should be identified and knowledge about effective infection prevention must be supplemented. There are two main methods for engineering the airborne transmission pathways of COVID-19: experimental and numerical approaches. Experiments need to prepare two real people, one corona-infected and the other non-infected. However, this is impractical because of the high risks for the non-infected person.

On the other hand, computational simulations can be conducted safely and easily without preparing any real subjects. In particular, computational fluid dynamics (CFD) has been used to assess the risk of airborne infectious diseases. For example, Yamakawa et al. [1] simulated influenza infection using a respiratory and lung model represented by unstructured and moving grids. They concluded that infection caused by

influenza viruses was more likely to occur with nasal breathing than with oral breathing. Ogura et al. [2] used the results of airflow simulations in a respiratory tract for modeling airflow in a room. The coupled simulations of flow fields in the room and in the respiratory tract made it possible to predict the motion of virus-laden droplets affected by coughing and breathing. The result showed that large droplets flew downward, and small droplets flew upward in the room. Additionally, most of the droplets inhaled through the nose adhered to the nasal cavity in the respiratory tract. Srivastav et al. [3] used a three-branched airway model to simulate particle deposition. In brief, most of the droplets were deposited at the bifurcation due to inertial impaction. However, they simulated moving virus-laden droplets only in the respiratory tract system. Moreover, the particle size and number of droplets adhered to the respiratory lining are not presented. Detailed information on droplets adhered to the respiratory lining can accurately assess the infection risk.

Therefore, this study used a human model with airways to calculate the behavior of the virus. In addition, we clarified the place where the droplets emitted during talking adhered to the opponent's respiratory lining. The diameter of the adhered droplets and the number of droplets were also measured.

2 Numerical Approach

2.1 Flow field and heat analysis

The flow and temperature fields were calculated by using the fluid simulation software *SCRYU/Tetra* [4]. The governing equations are the continuity equations, the incompressible Navier–Stokes equations, and the energy conservation equation. The continuity equation is defined by

$$\frac{\partial u_i}{\partial x_i} = 0. \quad (1)$$

The three-dimensional incompressible Navier–Stokes equations are given by

$$\frac{\partial(\rho u_i)}{\partial t} + \frac{\partial(u_j \rho u_i)}{\partial x_j} = -\frac{\partial p}{\partial x_i} + \frac{\partial}{\partial x_j} \mu \left(\frac{\partial u_i}{\partial x_j} + \frac{\partial u_j}{\partial x_i} \right) - \rho g_i \beta (T - T_0), \quad (2)$$

where $u_i (i, j = 1, 2, 3)$ represent the air velocity in the x , y , and z coordinates, and ρ indicates density, which is constant. t , p , and μ denote time, pressure, and viscosity coefficient, respectively. $g_i (i, j = 1, 2, 3)$ are the gravitational acceleration in the x , y , and z coordinates. β represent the body expansion coefficient. T and T_0 indicate temperature and base temperature, respectively. The energy conservation is defined by the following equation:

$$\frac{\partial(\rho C_p T)}{\partial t} + \frac{\partial(u_j \rho C_p T)}{\partial x_j} = \frac{\partial}{\partial x_j} \left(K \frac{\partial T}{\partial x_j} \right) + \dot{q}, \quad (3)$$

where C_p is the constant pressure specific heat. K represents the thermal conductivity, and \dot{q} denotes the heat flux. The SIMPLEC algorithm [5] was used to solve Eqs. (1) and (2), handling with the coupling of velocity and pressure. The second order MUSCL method [6] was applied to the convective terms of Eqs. (2) and (3). The standard $k-\varepsilon$ model is adopted as a RANS turbulence model since this study evaluates the main flow.

2.2 Movement of virus-laden droplets

Droplet motions are modeled by following the method described in the study by Yamakawa [7]. First, we define the equation of transient motion of the droplets. After that, the change in radius of droplets due to evaporation and coalescence between droplets are considered. The reference [7] used random numbers every second to evaluate whether the virus was active or not, and then, droplets of inactive virus are removed accordingly. However, this study determined the lifespan of each virus-laden droplet by using a random number at the beginning of the calculation in order to reduce the computational cost. The virus-laden droplets are removed as soon as their lifetimes were over. In addition, this study omitted the position vector of the droplets in Eq. (15) of the reference [7] because two floating virus-laden droplets are in close proximity when they coalesced. Thus, the position vectors h_1 and h_2 of the two droplets before coalescence and the position vector h_3 of the coalesced droplet are approximated by

$$h_1 \approx h_2 \approx h_3. \quad (4)$$

3 Simulation of droplets in the room and the respiratory tract

3.1 Numerical model

Figure 1 shows a model of two people sitting in a room and a magnified view of the computational grids for one person. The size of the room is $3.0\text{m} \times 3.0\text{m} \times 3.0\text{m}$ and the two people sit face to face. The distance between the mouths of the two people is defined as x [m]. This study simulated the following cases: $x = 0.75, 1.00, \text{ and } 1.25$. A $0.5\text{ m} \times 0.5\text{ m}$ air vent is installed at the top of the room. Four different models are used in this simulation, as shown in Table 1.

Table 1. Definition of model type

Model type	Conditions for wearing a mask
(A)	Neither person wears a mask.
(B)	Only the breathing person wears a mask.
(C)	Only the talking person wears a mask.
(D)	Both people wear masks.

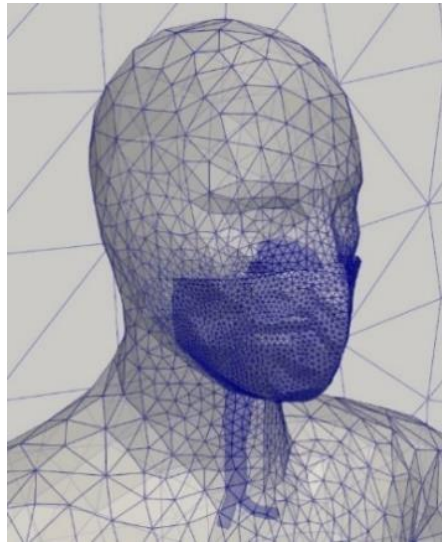
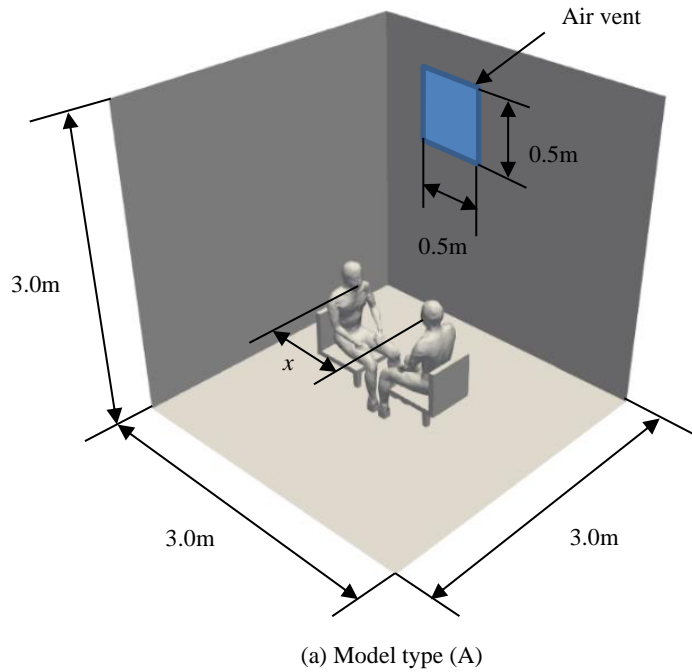
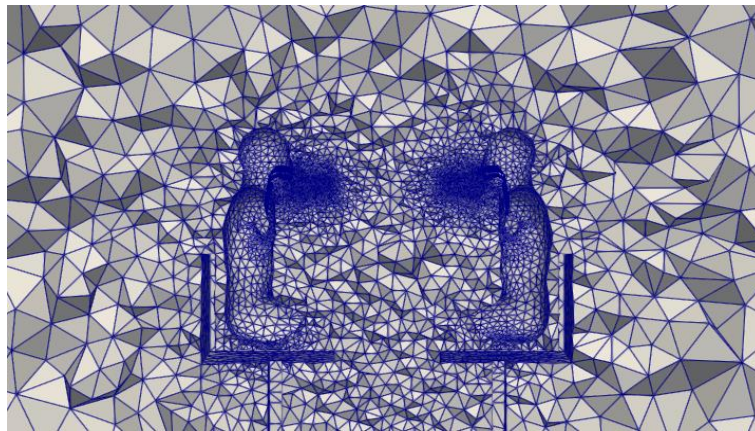
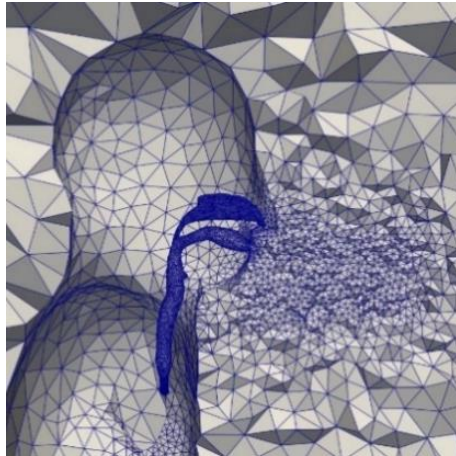


Fig. 1. Numerical model of the room and the human body with airway.

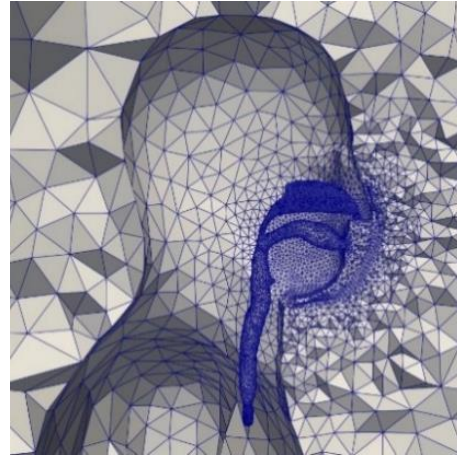
Figure 2 illustrates computational grids for the two human models, with (a) showing the sagittal plane, with (b) showing the cells around the face without a mask, and with (c) showing the cells around the mask. The grids were generated by *SCRYU/Tetra*. Figure 2(a) depicts the case where neither person wears a mask at $x = 0.75$. The surfaces of the airway and mask are covered with three prismatic layers. Computational grids are generated with approximately 1,000,000 cells for all the cases to reduce the computational cost. The smallest case involves 870,768 cells while the largest case includes 1,148,185 cells.



(a) Grid in sagittal plane



(b) Grid around the face without a mask



(c) Grid around the mask

Fig. 2. Grid around the human body with airways.

3.2 Computational conditions for flow analysis

Figure 3 shows the volume flow rate of breathing described in the Handbook of Physiology [8]. In this study, the positive volume flow rate represents intake air while the negative volume flow rate represents exhale air. This volume flow rate was given at the bronchial inlet surface of the breathing person as a boundary condition. Also, total pressure $p_T = 0$ was given at the air vent. The initial conditions are $p = 0.0$ and $u_1 = u_2 = u_3 = 0.0$.

In addition, Gupta et al. [9] defined the volume flow rate of talking, as shown in Fig. 4. This volume flow rate is given at the bronchial inlet surface of the talking person. The initial conditions are the same as the conditions for the breathing person. The talking person emits virus-laden droplets while the breathing person is exposed to the droplets. For other computational conditions, the room temperature is estimated to be $T_0 = 20^\circ\text{C}$. The exhalation/inhalation temperature and human body surface temperature are assumed to be $T_1 = 30^\circ\text{C}$.

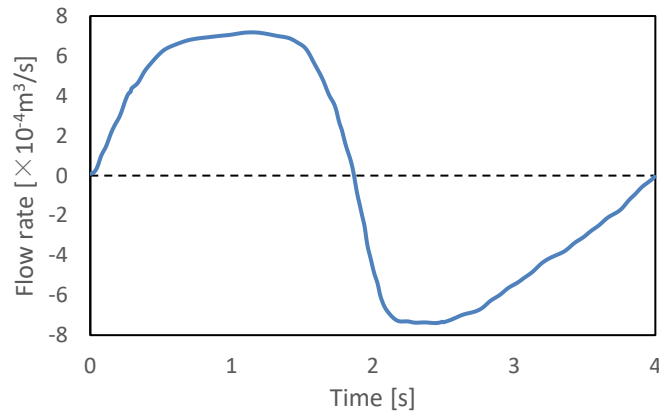


Fig. 3. Volume flow rate of breathing.

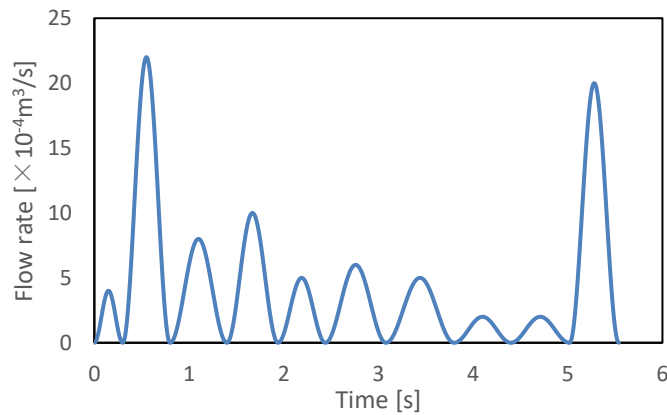


Fig. 4. Volume flow rate of talking.

3.3 Computational conditions for droplet analysis

Figure 5 shows the number distribution of droplets by diameter. This was determined from the literature of Duguid et al. [10] and Bale et al. [11]. The literatures also showed that about 9600 droplets are released during a one-minute speech. Therefore, this study generated 16 droplets every 0.1 seconds from the bronchial entrance and simulated for 60 seconds. Figure 6 shows the initial generating position of droplets, with eight droplets generated on each side.

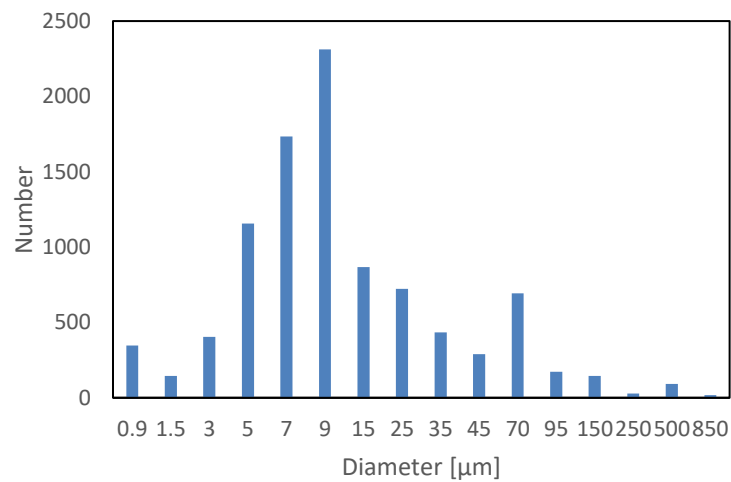


Fig. 5. Diameter and number distribution of droplets emitted during talking.

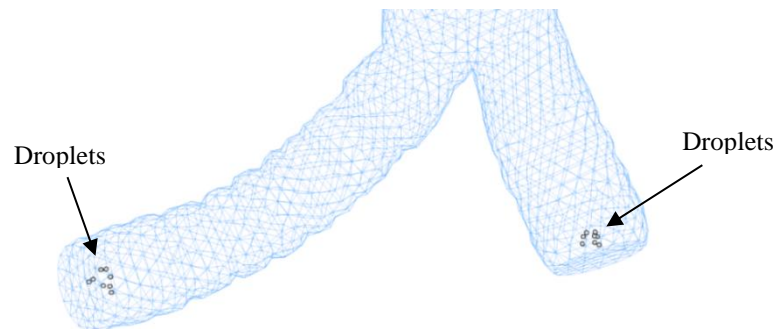


Fig. 6. Initial position for generating droplets.

The number and diameter of droplets adhered to the respiratory lining were examined as well. As shown in Fig. 7, the respiratory tract was divided into four regions: noses, mouth, trachea, and bronchi. The number and diameter of droplets adhered within each region, as well as to the bronchial inlet surface, were examined.

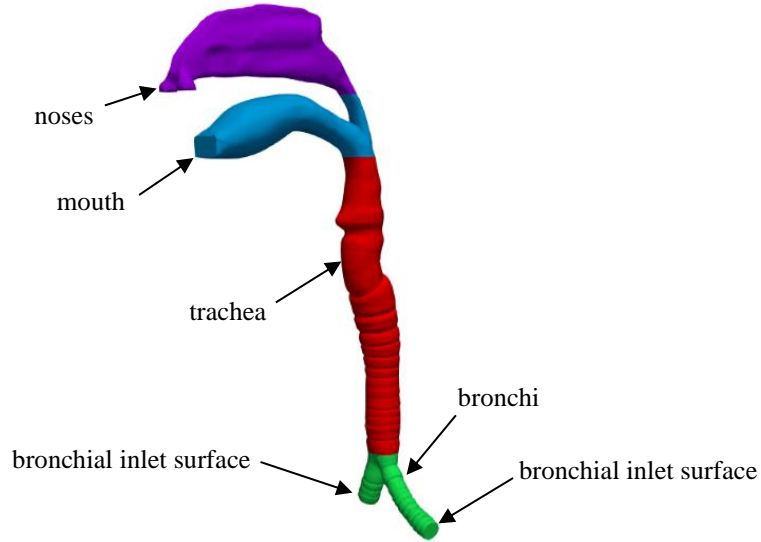


Fig. 7. The areas where droplets are counted.

3.4 Results of droplet analysis and discussion

Table 2 shows the number of droplets which the breathing human aspirated, with the percentage of droplets adhered to the bronchial inlet surface in the total aspirated droplets. No droplets inhaled by the breathing person was observed in model type (C) and (D). The highest number of aspirated droplets was obtained at $x = 1.25$ in model (A). It is notable that the number of aspirated droplets at $x = 1.00$ in model (B) was higher than that in model (A). In addition, more than 80% of the droplets adhered to the bronchial inlet surface. In summary, the effective way to reduce the number of droplets inhaled by the breathing person is wearing a mask by the talking person. On the other hand, wearing a mask by only the breathing person could not completely block droplets emitted by the talking person.

Table 2. The number of aspirated droplets in the airway of the breathing human.

Model type	x [m]	Number of aspirated droplets	Number of droplets adhered to the bronchial inlet surface	Proportion [%]
(A)	0.75	70	63	90.0
	1.00	61	53	86.9
	1.25	89	72	80.9
(B)	0.75	64	59	92.2
	1.00	91	78	85.7
	1.25	33	31	93.9

Figure 8 shows the streamlines at $x = 1.00$ and $t = 1.1$ in model (B), when the volume flow rate of inhalation peaked. It can be seen that the flow from the outside to the inside of the mask slightly facilitates the suction of droplets, which leads to the entry of droplets into the airway at $x = 1.00$ in model (B). However, this phenomenon was not observed in other cases, thus the sufficient number of samples should be necessary to analyze it.

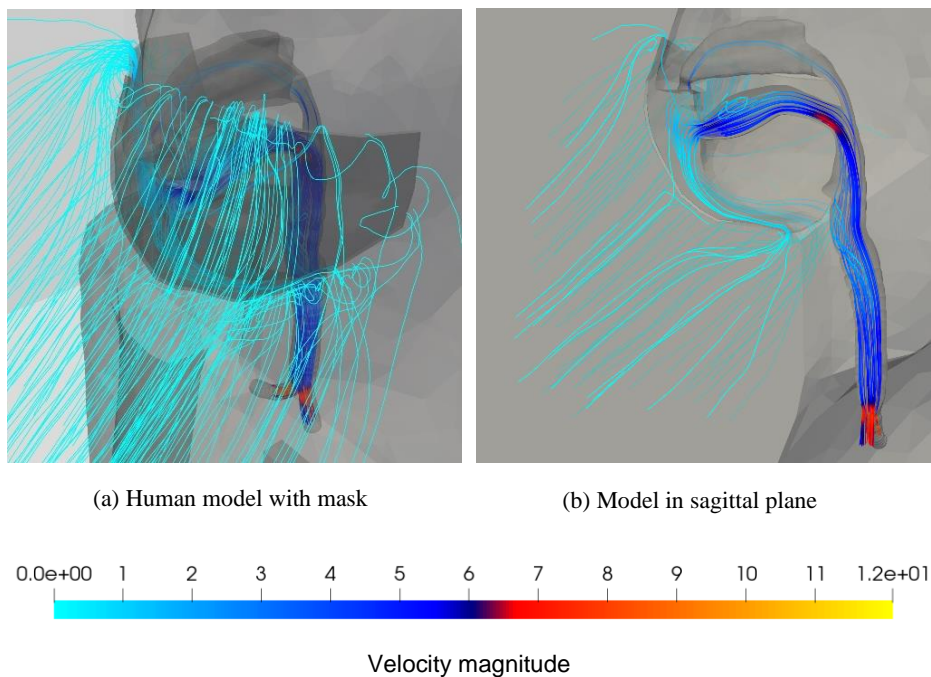
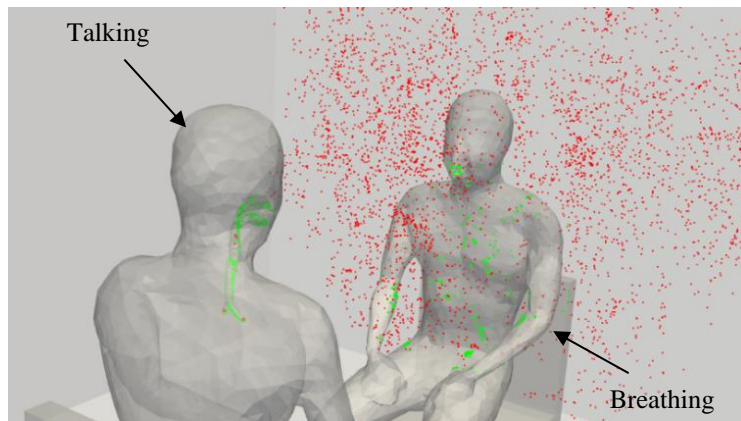
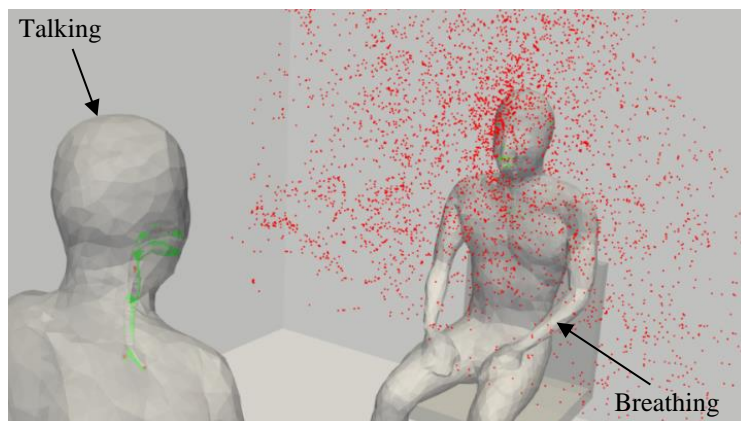


Fig. 8. Streamline at $x = 1.00$, $t = 1.1$ in model (B).

Figure 9 shows the distribution of droplets in model (A). The red particles represent floating droplets while the green particles represent adhered droplets. The droplets are released slightly downward due to the shape of the mouth. In addition, there is an up-draft around the people due to the body heat, making the droplets prone to rise. However, many droplets adhere to the conversation partner's torso at $x = 0.75$ because the distance between the two people was too short for droplets to rise. On the other hand, many droplets are carried to the partner's mouth at $x = 1.25$.

(a) $x = 0.75, t = 0.2$ (b) $x = 0.75, t = 60.0$ (c) $x = 1.25, t = 60.0$ **Fig. 9.** Droplets distribution in model (A).

Figures 10 and 11 show the numbers of droplets adhered to the respiratory lining in model (A) and in model (B), respectively. Figures 10(a) and 11(a) indicate that droplets larger than $35\ \mu\text{m}$ adhered to nowhere. In addition, the adhered droplets increase at the diameters of $7\ \mu\text{m}$ and $9\ \mu\text{m}$. The number distribution in Figs. 10(a) and 11(a) can be said to be reasonable, considering that the number of particles emitted during talking becomes high at the diameter of $7\ \mu\text{m}$ and $9\ \mu\text{m}$, as illustrated in Fig. 5.

Figures 10(b) and 11(b) show the number of droplets adhered to the bronchial inlet surface. It can be seen that most of the aspirated droplets adhered to the bronchial inlet surface, compared with Figs. 10(a) and 11(a). The number of droplets adhered to the bronchial inlet surface was considerably high at $x = 1.00$ in Fig. 11(b). It can be considered that the flow from the outside into the mask accelerates the speed of droplets, and thus, they gained a high enough speed to reach the bronchial inlet surface.

Figures 10(c) and 11(c) indicate that a substantial number of droplets adhered to the bronchi compared to the other areas, which means that few droplets adhered to the areas other than the bronchi. The highest number of droplets adhered to the trachea was observed at $x = 1.00$, as shown in Fig. 10(d), while only one droplet adhered at $x = 0.75$ in Fig. 11(d). The number did not tend to increase at the diameters of $7\ \mu\text{m}$ and $9\ \mu\text{m}$ at trachea.

At the mouth in Fig. 10(e), the number of adhered droplets with the diameter of $15\ \mu\text{m}$ peaked at $x = 1.25$. In contrast, in Fig. 11(e), only one droplet with the diameter of $3\ \mu\text{m}$ adhered to the mouth at $x = 1.25$. Droplets adhered to the nose only when $x = 1.25$ in Fig. 10(f), while the adhesion was observed when $x = 1.00$ as well in Fig. 11(f). Not as many droplets adhered to the mouth and nose in model (B) as model (A). This suggests that the mask prevented droplet aspiration.

Droplets adhered only to the area deeper than the mouth at $x = 0.75$ and $x = 1.00$ in Figs. 10(c) and 10(d) while when $x = 1.25$ can observe droplet adhesion to the mouth and nose in Figs. 10(e) and 10(f). This implies that at $x = 1.25$, the droplets emitted during talking decelerate because the distance between the two people was too far, and thus, they lost power to reach the partner's area deeper than mouth.

4 Conclusions

This study simulated virus-laden droplets that are transmitted from lung to lung. Fluid flow and droplet behavior were analyzed for 12 models. In summary, the following three conclusions were obtained: First, most of the droplets aspirated by the breathing person adhered to the bronchial inlet surface. Second, droplets with a large diameter did not reach the inner wall of the airway. Third, the droplets adhered to the conversation partner's torso because of the insufficiently short distance for them to rise. This study will apply to various cases by changing computational conditions and model configurations.

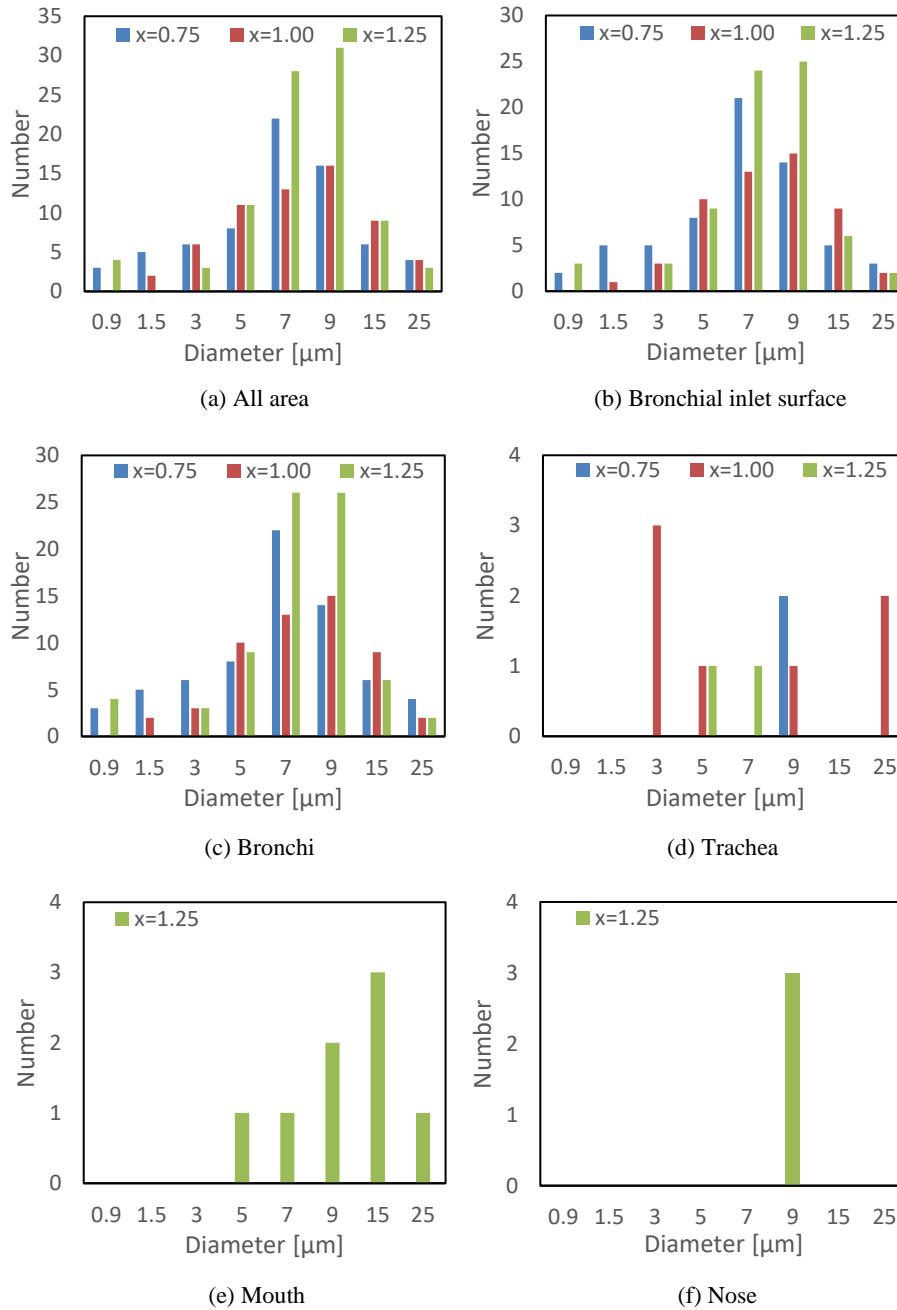


Fig. 10. The number distribution of droplets adhered to the respiratory lining in model (A).

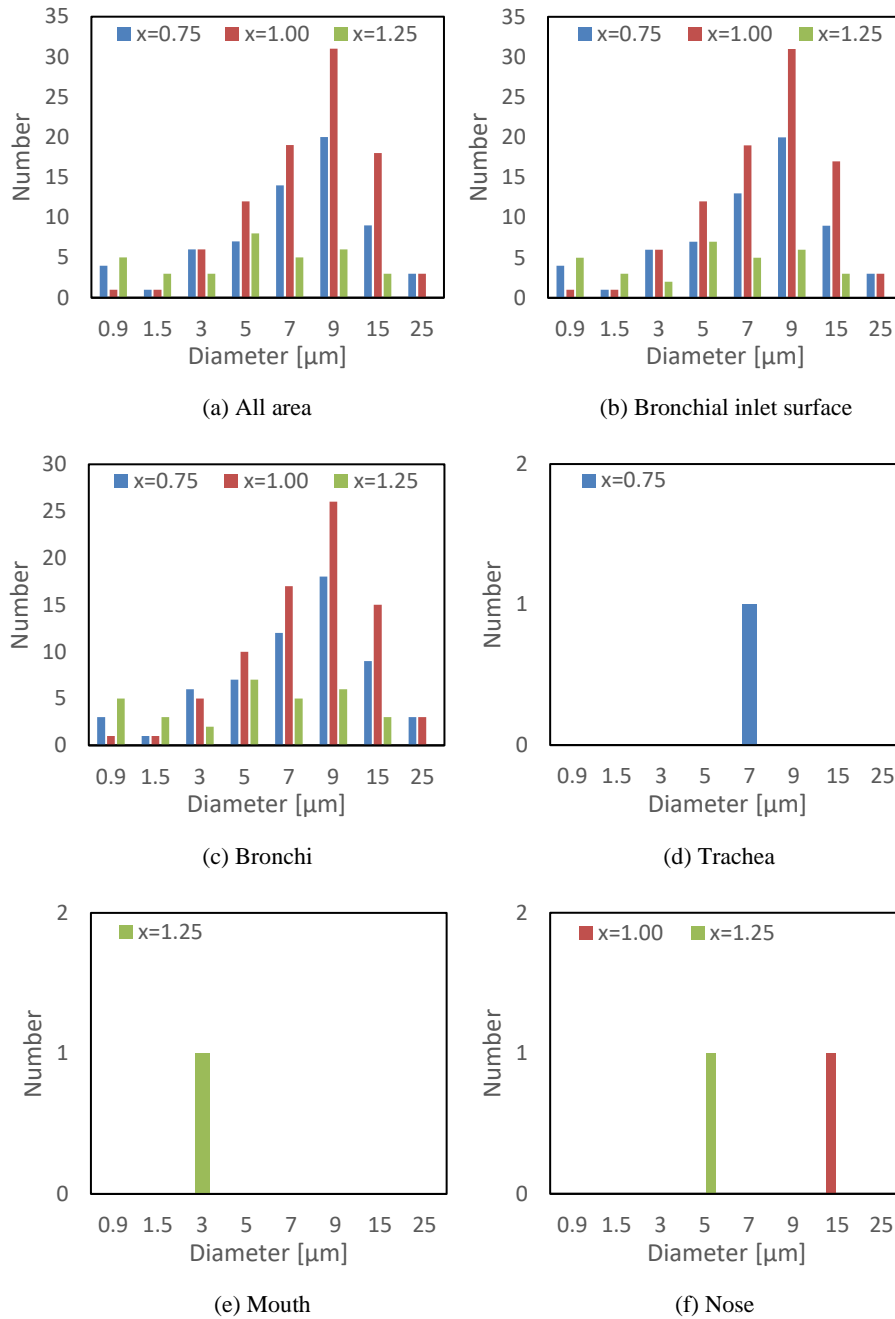


Fig. 11. The number distribution of droplets adhered to the respiratory lining in model (B).

Acknowledgments. This work was supported by JST CREST Grant Number JPMJCR20H7, by JKA through its promotion funds from KEIRIN RACE, and by JSPS KAKENHI Grant Number 21K03856.

References

1. Yamakawa, M., et al.: Influenza Viral Infection Simulation in Human Respiratory Tract. In: The Proceedings of 29th International Symposium on Transport Phenomena, Paper ID:13, Honolulu Hawaii (2018).
2. Ogura, K., et al.: Coupled simulation of Influenza virus between inside and outside the body. In: The Proceedings of the International Conference on Computational Methods, Vol.7, 71–82 (2020).
3. Srivastav, V., et al.: CFD Simulation of Airflow and Particle Deposition in Third to Sixth Generation Human Respiratory Tract. Proceedings of 39th National Conference on Fluid Mechanics & Fluid Power, SVNIT Surat, Gujarat, India, Vol.227, (2012).
4. Watanabe, N., et al.: An 1D-3D Integrating Numerical Simulation for Engine Cooling Problem. SAE Technical Paper 2006-01-1603, (2006).
5. Doormal, V.J.P., Raithby, G.D.: Enhancements of the simple method for predicting incompressible fluid flows. Numerical Heat Transfer, Vol.7, No.2, 147–163 (1984).
6. van Leer, B.: Towards the Ultimate Conservation Difference Scheme 4: A New Approach to Numerical Convection. J.Comp. Phys., 23, 276–99 (1977).
7. Yamakawa, M. et al.: Computational investigation of prolonged airborne dispersion of novel coronavirus-laden droplets. Journal of Aerosol Science. Volume 155, 105769 (2021).
8. Fenn, W. O., Rahn, H.: Handbook of Physiology, Section3: Respiration, American Physiological Society Washington DC (1965).
9. Gupta, J. K., et al.: Characterizing Exhaled Airflow from Breathing and Talking. Indoor Air 20.1 (2010).
10. Duguid, J. P., et al.: The size and the duration of air-carriage of respiratory droplets and droplet-nuclei. Epidemiology & Infection 44, 6, 471–479 (1946).
11. Bale, R., et al.: Simulation of droplet dispersion in COVID-19 type pandemics on Fugaku. PASC'21, Article No.4, 1–11 (2021).